Title
Broadband continuous single-mode tuning of a short-cavity quantum-cascade VECSEL

Journal
Nature Photonics, 13(12)

ISSN
1749-4885

Authors
Curwen, CA
Reno, JL
Williams, BS

Publication Date
2019-12-01

DOI
10.1038/s41566-019-0518-z

Peer reviewed

Title: Broadband continuous single-mode tuning of a short-cavity quantum-cascade VECSEL

Authors:

Christopher A. Curwen[1] (ccurwen@ucla.edu), John L. Reno[2] (jlreno@sandia.gov), Benjamin S. Williams[1,*] (bswilliams@ucla.edu)

[1]Department of Electrical and Computer Engineering, University of California Los Angeles, Los Angeles, CA 90095, USA

[2]Sandia National Laboratories, Center of Integrated Nanotechnologies, MS 1303, Albuquerque, New Mexico 87185, USA

*Indicates corresponding author

Introduction paragraph:

Changing the length of a laser cavity is a simple technique for continuously tuning the wavelength of a laser but is rarely used for broad fractional tuning, with a notable exception of the diode laser VCSEL[1,2]. This is because, to avoid mode hopping, the cavity must be kept optically short to ensure a large free-spectral-range (FSR) compared to the gain bandwidth of the amplifying material. Terahertz quantum-cascade (QC) lasers are ideal candidates for such a short cavity scheme as they demonstrate exceptional gain bandwidths (up to octave spanning)[3] and can be integrated with broadband amplifying metasurfaces.[4] We present such a QC-metasurface based vertical-external-cavity surface-emitting-laser (VECSEL) that exhibits over 20% continuous fractional tuning of a single laser mode. Such tuning is possible because the metasurface has sub-wavelength thickness which allows lasing on low-order Fabry-Pérot cavity modes. Good beam quality and high output power are simultaneously obtained.

Main text:

Widely tunable, single-mode laser sources are of interest for myriad applications, including broadband spectroscopy, frequency-agile heterodyne receivers, and optical coherence tomography[5,6]. While there are countless specific techniques for tuning laser emission[7-9], most can be categorised by modeling the laser as a simple Fabry-Pérot (FP) cavity oscillating at a frequency $v_m = mc/2nL$. The order of the longitudinal mode is given by m, L is the physical length of the cavity, and n is the index of refraction of the constituent medium (or modal effective index in the case of a waveguide). Tuning the frequency over a range δv occurs through some combination of tuning n, m, or L; continuous tuning requires control of n or L. Changing the index n – for example using temperature – usually provides fractional tuning $\delta v/v$ of not more than 1% since the achievable $\delta n/n$ is similarly small for most laser materials. Use of monolithic sampled-grating or coupled-cavity approaches can increase tuning ranges to a few percent by stitching together tuning regimes[10-12]. Changing the cavity length L also provides limited tunability since laser cavities are typically orders of magnitude longer than their lasing wavelengths, which results in a small tuning range $\delta v \approx$ FSR before mode-hopping occurs. In most cases, broadband tuning is accomplished by introducing tunable intracavity spectral filters such as gratings, etalons, prisms, etc. These techniques typically amount to hopping between longitudinal modes m, while continuous tuning between modes can often be obtained with fine control of L. If enough parameters are synchronously tuned, tracking of a mode with constant m over broad bandwidths can be often be recovered[13,14], but such approaches require careful design and are often limited in speed and repeatability. Laser sources based on nonlinear optical processes, such as optical parametric oscillators and

Raman lasers[15,16], have additional controls in pump frequency and phase matching conditions that allow for extremely broad tunability, however they are beyond the intended scope of this discussion.

Broadly tuning a laser's wavelength using only control of the cavity length L is possible if the laser resonator can be made extremely short, which forces it to operate on a low-order longitudinal mode ($\delta\nu/\nu = 1/(m+1/2)$ in a simple FP cavity). This is a difficult criterion for most lasers as such a short cavity requires very highly reflective mirrors to compensate for the short propagation length within the gain medium. Swept-wavelength VCSELs, which use high-reflectivity MEMS mirrors to allow cavity lengths of only a few wavelengths, are perhaps the only successful realization of broadband continuous tuning using L (up to 10% demonstrated)[17,18].

Here, we present broad, continuous tuning of a short external cavity laser based on the recently reported THz quantum-cascade vertical-external-cavity surface-emitting-laser (QC-VECSEL)[4,19]. Quantum-cascade (QC) lasers are particularly appealing for broadband tuning as the gain material can be engineered to exhibit up to octave spanning bandwidths[3]. Mid-IR QC-lasers have demonstrated up to 39% fractional tuning around 9.5 μm using external cavity (EC) Littrow configurations with heterogeneous stacks of QC-gain material[20]. However THz QC-lasers are more challenging to implement in EC configurations because the sub-wavelength sized metal waveguide resonators exhibit extremely poor coupling to free space, which makes it difficult to create effective anti-reflective coatings on the waveguide facets. The most successful examples are EC lasers based on QC surface-plasmon waveguides with facet-mounted silicon lenses[21,22] (~4% fractional tuning), and EC coupling to a metal-metal waveguide second-order distributed feedback grating[23,24] (~5% fractional tuning). As a result, researchers have turned to more exotic schemes, such as perturbation of the evanescent fringing field of a metal-metal wire laser using a MEMS "plunger"[25]. This approach has demonstrated up to 8.6% fractional continuous tuning around 3.85 THz, but due to its subwavelength radiating aperture, the beam quality is poor, and the output power is low[26,27].

This work demonstrates that the QC-VECSEL architecture allows for broadband tuning while simultaneously providing high power and good beam quality. The enabling component is an amplifying reflectarray metasurface made up of narrow metal-metal ridge waveguides loaded with THz QC gain material. The ridges are spaced with subwavelength periodicity ($\Lambda < \lambda_0$) and are coupled to surface incident radiation on a unit-cell basis via the TM_{01} transverse cutoff resonance centred at $\nu_o \approx c/(2nw)$, where w is the width of the ridges. At the cutoff frequency, there is no propagation or phase variation along the length of the ridges, and the odd symmetry of the vertical sidewall fields results in constructive interference of radiation in the surface direction. When electrical bias is applied to the metasurface, the THz QC gain material provides reflective amplification via stimulated emission. This metasurface is used as the gain chip in an external cavity laser; the concept is illustrated in Fig. 1. The advantage of the QC-VECSEL approach is that the radiating aperture of the metasurface is millimeter scale (rather than micron scale for a facet emitting device) which allows generation of high-power, directive, and near-diffraction limited beams[28-30]. Further, by oscillating on low-order FP cavity modes (as low as m=2 shown here), continuous tuning over large fractional bandwidths can be achieved via mechanical control of the cavity length. The QC-VECSEL is an excellent candidate for short-cavity configurations because the gain is based on a per-reflection basis rather than a per-unit-length basis, so reducing the cavity length has no adverse effect on the laser threshold. While the metasurface does have a physical thickness (10 μm ridge height), it is thin compared to the free space wavelength (as short as 85 μm), which allows for subwavelength sized cavities. The metasurface in this experiment is designed to be resonant at 3.5 THz and consists of an array of ridges of width w = 11.9 μm repeated with a period of Λ = 41.7 μm. The metasurface is spatially uniform across the 1.5×1.5 mm^2 area, although only a central circular area 0.5 mm in diameter is electrically biased in order to preferentially pump the fundamental Gaussian mode. The simulated metasurface reflectance and reflection phase is shown in Fig. 1b, along with that from a comparison metasurface with Λ=70 μm. The smaller period device exhibits broader bandwidth at the expense of peak gain (see Ref. [19]). The lower amplification factor makes the VECSEL more sensitive to diffraction and outcoupling losses, but these factors can be mitigated with proper choice of output coupler and use of very short cavities (see Supplemental Section S3).

The resonant modes of the QC-VECSEL cavity are given by the condition:

$$2kL_{EC} - \varphi_{meta} - \varphi_{OC} = 2\pi m \qquad (1)$$

Where $k=2\pi v/c$ is the free space wavenumber, L_{EC} is the length of the external cavity, and φ_{meta} and φ_{oc} are the frequency dependent reflection phases of the metasurface and output coupler respectively. In a simple cavity, where the phase terms have no frequency dependence, by operating on the m = 1 mode, up to an octave of single-mode tuning (equivalent to 66% fractional tuning) can be achieved since $v_{m=2} = 2v_{m=1}$ (assuming symmetric operation around a homogeneously broadened gain curve). In this work, while $\varphi_{oc} \approx \pi$ with little spectral dependence (see Supplementary Section S2), φ_{meta} exhibits nearly 2π phase shift across the resonance (Fig. 1b). This phase accumulation represents a group delay ($\tau_g = d\varphi_{meta}/d\omega$), which has the effect of compressing the FSR near resonance and reducing the maximum single-mode tuning range for a given order m. This effect can be seen in Fig. 1d, where the cavity mode frequencies are plotted including the effects of metasurface phase. Based on the figure, the best case for single-mode tuning is ~24% fractional, and in fact occurs on the m=2 mode. In theory, even larger tuning should be attainable by operating on the m=1 mode, but in practice the physical thickness of the metasurface ridges limits the cavity length to a minimum of 10 μm, which prevents this mode from tuning to frequencies higher than ~3.7 THz.

Experimentally, the tunable VECSEL cavity was constructed entirely within a vacuum cryostat, and a piezoelectric stepper motor was used to control the position of the output coupler (Supplemental Section S1). Results of tuning on the m=4 mode of the cavity are presented in Fig. 2. Up to 650 GHz of continuous, single-mode tuning is observed, centred around 3.47 THz (19% fractional tuning). A consistent, circular beam pattern with a FWHM divergence angle of ~15° is observed throughout the tuning range (Fig. 2b). The peak power and slope efficiency of the VECSEL is plotted in Fig. 2e for pulsed mode operation and in Fig. 2f for continuous-wave operation (see Supplemental Section S4 for extended data). The threshold and peak current densities (J_{th} and J_{pk} respectively) are plotted in Fig. 2d. The variations in power, slope efficiency, and threshold that are seen in Figs. 2d,e,f are primarily a result of the changing output coupler reflectance (see Ref [19]). At the edges of the tuning range, the VECSEL lasing frequency becomes bias dependent, hopping from the low frequency resonance of the cavity to the high frequency resonance when the bias voltage is increased (Fig. 2h); the two modes are not observed to lase simultaneously. Such behavior is consistent with the Stark shift of intersubband transitions with applied field and/or the contribution of multiple intersubband transitions to the gain spectra for this active material[31]. Neither the length of the external cavity, nor the relative position of the output coupler can be measured directly with the equipment available, but this information can be inferred from the observed FSR at the edges of the tuning range. The observed FSR at the longest and shortest cavity lengths was 500 GHz (3.18 – 3.68 THz) and 610 GHz (3.79 – 3.18 THz) respectively, and using equation (1), the inferred change in cavity length is 177 - 130 μm. The resonant frequencies and FSR predicted by equation (1) match very well (<1% difference) with the experimentally observed values, indicating that the fabricated device behaves very close to the simulated design.

To push for maximum tuning, the length of the cavity was further reduced to operate on the m=2 mode. 25.1% fractional tuning was achieved from 3.11 – 3.99 THz as the cavity length was varied from 86 – 48 μm (Figure 4). However, for such short cavities, higher order beams are regularly observed, and multimoding begins to occur at the shortest cavity lengths. This is a result of the modal spot sizes on the metasurface shrinking with the length of the external cavity, which reduces the threshold for competing higher order modes (see Supplemental Section S3). It is likely that this issue can be managed in the future by reducing the bias diameter on the metasurface to increase the selectivity over higher-order modes, albeit with the trade-off of increased threshold gain values. Below L_{EC}=48 μm, the threshold current increases quickly until lasing ceases. This could be caused by contact between the output coupler stage and the metasurface mount resulting in sudden cavity misalignment; at such short cavity lengths, a cavity misalignment of only 0.1° would cause contact between the outer edges of the mount (which is 3 cm wide, see Supplemental Section S1). This explanation would also be consistent with the significantly degraded beam pattern of Fig. 3(d).

In conclusion, we have shown that the QC-VECSEL architecture allows realization of short-cavity single-mode lasers, continuously tunable over more than 20% fractional bandwidth. Furthermore, the approach does not sacrifice laser performance; the reported continuous-wave power and wall-plug efficiencies are high for THz QC-lasers, and high quality beam patterns are maintained throughout. The key enabling technology is the active reflectarray metasurface; not only does it sidestep the issue of antireflective facet coatings, but its optically thin profile allows lasing on very low-order longitudinal modes (as low as m=2) of the external cavity. The primary limiting factor for the tuning range is the phase response of the metasurface. Paths towards even broader tunability include phase engineering of both the metasurface and output coupler, and development of thinner metasurfaces to push the ultimate limits of tuning with cavity length on the m=1 mode. Further improvements to device performance and reliability could include development of broadband, spectrally flat output couplers, and monolithic integration of the output coupler using MEMS technology.

Methods

Electromagnetic simulations

Finite element (FEM) electromagnetic simulations were performed using COMSOL Multiphysics. Infinite metasurface reflectance spectra were simulated in a 2-D space using Floquet periodic boundary conditions. Metal and semiconductor material losses were estimated using the Drude model. FEM eigenmode simulations were also performed on 2-D VECSEL cavities to study the influence of diffraction on threshold gain (Supplemental Section S3). These simulations are verified using numerical Fox and Li calculations done in MATLAB.

P-I-V, power, spectral, and beam pattern measurements

All measurements were performed at a heat-sink temperature of 77 K on a cold stage within a vacuum cryostat. The cryostat window was 3.3-mm-thick high-resistivity silicon with an anti-reflective parylene coating deposited on each side and measured to have a ~90% transmittance between 3-4 THz. The laser was tested in pulsed and continuous wave modes. Pulsed measurements were performed at 1% duty cycle with a 10 kHz repetition rate. Relative output power was measured using a pyroelectric detector (GentecEO), and absolute power levels were directly measured with a calorimeter (Scientech) that was calibrated against a Thomas Keating absolute terahertz power meter. Reported powers refer to the emitted laser power, having accounted for the measured transmittance of the cryostat window. Far-field beam patterns were measured using a 2-axis scanning pyroelectric detector with a 2 mm diameter aperture rotating at a constant distance ≈15 cm from the device. Spectra were measured using a Fourier-transform infrared-spectrometer (FTIR, Nicolet 8700) and a DTGS pyroelectric detector.

Piezoelectric cavity length tuning

The metasurface was mounted to a fixed copper block, while the output coupler was mounted on a single-axis piezoelectric stepping stage (Attocube ANPx311, Supplemental section S1). The piezoelectric stepper is operated in an open loop mode without position readout, so the relative output coupler position cannot be directly determined. Continuous cavity length actuation is also available between steps.

Output couplers

The output coupler was made by depositing a Ti/Au metallic inductive mesh (10 μm pitch, 3 μm wire width) on a 133 μm thick z-cut crystal quartz wafer. It is designed to provide a relatively high reflectance to minimise the threshold gain and maximise the tuning range. The measured transmission spectrum is shown in Fig. 2c. See Supplemental Section S2 for analysis of output coupler losses on the performance of the QC-VECSEL, and Supplemental Section S5 for the effect of using a lower reflectance output coupler on tuning.

Active region gain medium

The quantum-cascade active region design used for this study consists of an $Al_{0.15}Ga_{0.85}As/GaAs$ heterostructure where, starting from the injection barrier, the layer thicknesses in Å are **51**/103/**17**/107/**37**/88/**37**/<u>172</u> (barrier layers are bold). The central 88 Å of the underlined well is Si-doped at 5×10^{16} cm^{-1}. The design is almost identical to that in Ref. [32], and is based on the hybrid bound-to-continuum/resonant-phonon concept presented in Ref. [33]. The design has been reported to provide high power levels and robust, broadband behavior. The metasurface was made from the same wafer used in Refs. [28] and [29] (wafer number VB0739). The maximum pulsed-mode operating temperature has been measured to be 170 K in a metal-metal ridge waveguide and 130 K for a VECSEL using a highly reflective output coupler (>95% reflectance)[30]. Previous measurements observed continuous gain between 2.9 and 4.0 THz.

Fabrication

Fabrication was performed using the standard metal-metal waveguide procedure outlined in Ref. [34]. The process began with deposition of Ti/Cu :: 10/300 nm on the active QC sample and a receiving doped piece of GaAs. Thermocompressive wafer bonding was performed, and the QC wafer substrate was removed via mechanical polishing and subsequent wet etching. The highly doped 100 nm of GaAs that is typically used for improving electrical contact is removed as to reduce current spreading into unbiased portions of the metasurface. Next, a PECVD oxide layer is deposited to provide selective bias, top Ti/Au :: 15/250 nm contacts are deposited along with a self-aligned 200 nm Ni mask, and 10 μm ridges are dry etched using ICP-RIE technology. Last, the remaining Ni mask is removed via wet etching, and a bottom contact is deposited on the backside of the substrate.

Acknowledgements:

This work was supported by the National Science Foundation (NSF) (1150071, 1407711, 1711892) and the National Aeronautics and Space Administration (NASA) (NNX16AC73G). This work was performed, in part, at the Center for Integrated Nanotechnologies, an Office of Science User Facility operated for the U.S. Department of Energy (DOE) Office of Science. Microfabrication was performed at the UCLA Nanoelectronics Research Facility, and wire bonding was performed at the UCLA Center for High Frequency Electronics. This work was performed, in part, at the Center for Integrated Nanotechnologies, an Office of Science User Facility operated for the U.S. Department of Energy (DOE) Office of Science. Sandia National Laboratories is a multi-mission laboratory managed and operated by National Technology and Engineering Solutions of Sandia, LLC., a wholly owned subsidiary of Honeywell International, Inc., for the U.S. DOE's National Nuclear Security Administration under contract DE-NA-0003525. The views expressed in the article do not necessarily represent the views of the U.S. DOE or the United States Government.

Author contributions:

C.A.C. and B.S.W. conceived of the idea. C.A.C. derived the experimental strategy, fabricated the devices, performed the measurements, and analyzed the data. J.L.R. performed the molecular beam epitaxy growth. C.A.C. and B.S.W. co-wrote the manuscript. All work was done under the supervision of B.S.W.

Competing Interests:

The authors declare no competing interests.

Data Availability Statement:

The data that support the plots within this study are available from the corresponding author upon reasonable request.

References:

1 Wu, M.S., Vail, E.C., Li, G.S., Yuen, W. & Chang-Hasnain, C.J. Tunable micromachined vertical-cavity surface-emitting laser. *Electron. Lett.* **31**, 1671-1672 (1995).

2 Huang, M.C.Y., Zhou, Y. & Chang-Hasnain, C.J. A nanoelectromechanical tunable laser. *Nat. Photon.* **2**, 180-184 (2008).

3 Rosch, M., Scalari, G., Beck, M. & Faist, J. Octave-spanning semiconductor laser. *Nat. Photon.* **9**, 42-47 (2015).

4 Xu, L.Y. *et al.* Metasurface external cavity laser. *Appl. Phys. Lett.* **107** (2015).

5 Jayaraman, V. *et al.* OCT Imaging up to 760 kHz Axial Scan Rate Using Single-Mode 1310nm MEMS-Tunable VCSELs with > 100nm Tuning Range. *Conf. Laser Electr.* (2011).

6 Lee, A.W.M., Kao, T.Y., Burghoff, D., Hu, Q. & Reno, J.L. Terahertz tomography using quantum-cascade lasers. *Opt. Lett.* **37**, 217-219 (2012).

7 Coldren, L.A. *et al.* Tunable semiconductor lasers: A tutorial. *J. Light. Technol.* **22**, 193-202 (2004).

8 Duarte, F.J. *Tunable laser optics*. Second edition. edn, (CRC Press : Taylor & Francis Group, 2015).

9 Godard, A. Infrared (2-12 μm) solid-state laser sources: a review. *Comptes Rendus Phys.* **8**, 1100-1128 (2007).

10 Jayaraman, V., Chuang, Z.M. & Coldren, L.A. Theory, design, and performance of extended tuning range semiconductor-lasers with sampled gratings. *IEEE J. Quantum Elect.* **29**, 1824-1834 (1993).

11 Kundu, I. *et al.* Quasi-continuous frequency tunable terahertz quantum cascade lasers with coupled cavity and integrated photonic lattice. *Opt. Express* **25**, 486-496 (2017).

12 Slivken, S. *et al.* Sampled grating, distributed feedback quantum cascade lasers with broad tunability and continuous operation at room temperature. *Appl. Phys. Lett.* **100** (2012).

13 Liu, A.Q. & Zhang, X.M. A review of MEMS external-cavity tunable lasers. *J. Micromechanics Microengineering* **17**, R1-R13 (2007).

14 Wysocki, G. *et al.* Widely tunable mode-hop free external cavity quantum cascade lasers for high resolution spectroscopy and chemical sensing. *Appl Phys B-Lasers O* **92**, 305-311 (2008).

15 Turitsyn, S.K. *et al.* Random distributed feedback fibre laser. *Nat. Photon.* **4**, 231-235 (2010).

16 Vijayraghavan, K. *et al.* Broadly tunable terahertz generation in mid-infrared quantum cascade lasers. *Nat. Commun.* **4** (2013).

17 Jayaraman, V., Cole, G.D., Robertson, M., Uddin, A. & Cable, A. High-sweep-rate 1310 nm MEMS-VCSEL with 150 nm continuous tuning range. *Electron. Lett.* **48**, 867-868 (2012).

18 Qiao, P.F., Cook, K.T., Li, K. & Chang-Hasnain, C.J. Wavelength-swept VCSELs. *IEEE J. Sel. Top. Quantum Electron.* **23** (2017).

19 Xu, L.Y. *et al.* Terahertz metasurface quantum-cascade VECSELs: theory and performance. *IEEE J. Sel. Top. Quantum Electron.* **23** (2017).

20 Hugi, A. *et al.* External cavity quantum cascade laser tunable from 7.6 to 11.4 μm. *Appl. Phys. Lett.* **95** (2009).

21 Lee, A.W.M., Williams, B.S., Kumar, S., Hu, Q. & Reno, J.L. Tunable terahertz quantum cascade lasers with external gratings. *Opt. Lett.* **35**, 910-912 (2010).

22 Ren, Y. *et al.* Fast terahertz imaging using a quantum cascade amplifier. *Appl. Phys. Lett.* **107** (2015).

23 Castellano, F. *et al.* Tuning a microcavity-coupled terahertz laser. *Appl. Phys. Lett.* **107** (2015).

24 Mahler, L., Tredicucci, A., Beltram, F., Beere, H.E. & Ritchie, D.A. Tuning a distributed feedback laser with a coupled microcavity. *Opt. Express* **18**, 19185-19191 (2010).

25 Qin, Q., Williams, B.S., Kumar, S., Reno, J.L. & Hu, Q. Tuning a terahertz wire laser. *Nat. Photon.* **3**, 732-737 (2009).

26 Qin, Q., Reno, J.L. & Hu, Q. MEMS-based tunable terahertz wire-laser over 330GHz. *Opt. Lett.* **36**, 692-694 (2011).

27 Orlova, E.E. *et al.* Antenna model for wire lasers. *Phys Rev Lett* **96** (2006).

28 Curwen, C.A., Reno, J.L. & Williams, B.S. Terahertz quantum cascade VECSEL with watt-level output power. *Appl. Phys. Lett.* **113** (2018).

29 Xu, L.Y., Chen, D.G., Itoh, T., Reno, J.L. & Williams, B.S. Focusing metasurface quantum-cascade laser with a near diffraction-limited beam. *Opt. Express* **24**, 24117-24128 (2016).

30 Xu, L.Y., Curwen, C.A., Reno, J.L. & Williams, B.S. High performance terahertz metasurface quantum-cascade VECSEL with an intra-cryostat cavity. *Appl. Phys. Lett.* **111** (2017).

31 Burnett, B.A., Pan, A., Chui, C.O. & Williams, B.S. Robust density matrix simulation of terahertz quantum cascade lasers. *IEEE Trans. Terahertz Sci. Technol.* **8**, 492-501 (2018).

32 Li, L.H. *et al.* Terahertz quantum cascade lasers with > 1 W output powers. *Electron. Lett.* **50**, 309-310 (2014).

33 Amanti, M.I. *et al.* Bound-to-continuum terahertz quantum cascade laser with a single-quantum-well phonon extraction/injection stage. *New J. Phys.* **11** (2009).

34 Williams, B.S., Kumar, S., Hu, Q. & Reno, J.L. Operation of terahertz quantum-cascade lasers at 164 K in pulsed mode and at 117 K in continuous-wave mode. *Opt. Express* **13**, 3331-3339 (2005).

35 Gordon, I.E. *et al.* The HITRAN2016 molecular spectroscopic database. *J Quant Spectrosc Ra* **203**, 3-69 (2017).

Figure captions:

Fig. 1 Metasurface cavity design and electromagnetic simulations. **a**, SEM of fabricated device. Metasurface is 1.5×1.5 mm^2 with a period of 41.7 μm and a ridge width of 11.9 μm. Current is only injected into a circular central bias area 500 μm in diameter, indicated with a dashed line. **b,** Simulations of the metasurface reflectance and reflection phase spectra when 25 cm^{-1} of intersubband gain is added to the ridges. Two metasurface periods Λ are simulated for comparison. **c**, Finite-element 2-D eigenfrequency simulation of the TEM$_{00}$ mode in a full QC-VECSEL cavity with $L_{EC} \approx 1.75$ wavelengths long (mode m=4). **d**, Cavity eigenfrequencies vs. L_{EC} for both a bare Fabry-Pérot cavity neglecting reflection phase (dashed), and cavity modes including metasurface phase (solid). Coloured boxes indicate the particular cavity modes over which tuning is presented in this work. Insets show the E-field magnitude at the two extremes of the m=2 mode.

Fig. 2 Measurement results on longitudinal mode *m*=4 with 19% fractional tuning at 77 K. a, Single-mode FTIR spectra and **b**, beam patterns measured as the piezoelectric stage is stepped, tuning the VECSEL's external cavity length and lasing frequency. It is noted that the tuning is not linear with cavity length as the reflection phase of the metasurface is frequency dependent. **c**, Output coupler transmission measured using FTIR. **d**, Threshold and peak current density in pulsed-mode. **e**, Peak-pulsed and **f**, continuous wave power and slope efficiency as a function of lasing frequency. Faded curve in **e** indicates atmospheric transmission features within the demonstrated tuning range simulated from the HITRAN database.[35] **g**, Pulsed and continuous wave *P-I-V* curves taken at 3.75 THz, and **h**, pulsed *L-I-V* curve indicating two distinct lasing regions at 3.18 THz and 3.68 THz (separated by the cavity FSR).

Fig. 3 Measurement results on longitudinal mode *m*=2 with 25% fractional tuning at 77 K. a, FTIR spectra collected as the external cavity length is tuned. The region in which multimode lasing is observed is indicated by the blue shaded area. **b**-**d**, Selected spectra and beams taken between the longest cavity **b** and the shortest cavity **d**. The beam quality is observed to degrade at shorter cavity lengths and at high bias.

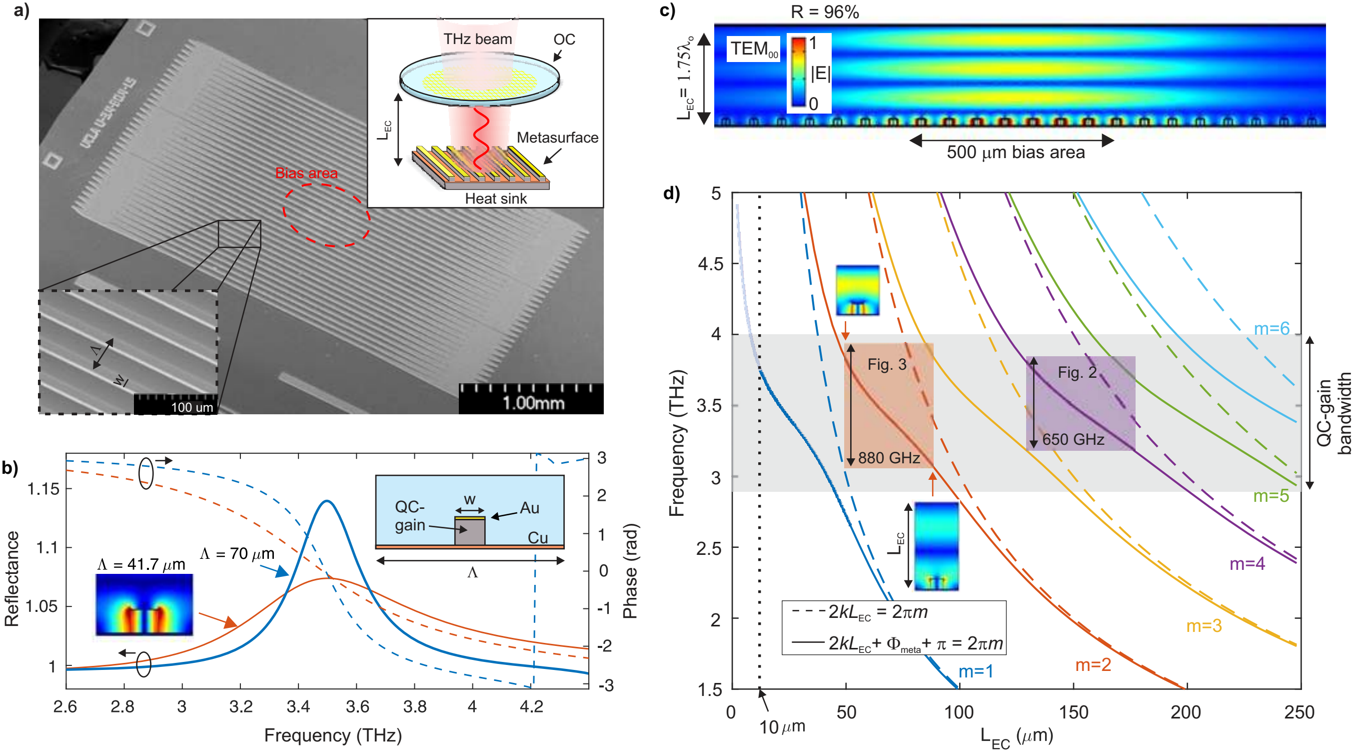
a)
UCLA U-3/1-5/31-15
Bias area
THz beam
OC
L_{EC}
Metasurface
Heat sink
Λ
w
100 um
1.00mm
b)
Reflectance
1.15
1.1
1.05
1
Phase (rad)
3
2
1
0
-1
-2
-3
Λ = 41.7 μm
Λ = 70 μm
QC-gain
w
Au
Cu
Λ
2.6
2.8
3
3.2
3.4
3.6
3.8
4
4.2
Frequency (THz)
c)
R = 96%
$L_{EC} = 1.75\lambda_o$
TEM_{00}
1
|E|
0
500 μm bias area
d)
Frequency (THz)
5
4.5
4
3.5
3
2.5
2
1.5
Fig. 3
880 GHz
Fig. 2
650 GHz
m=6
m=5
m=4
m=3
m=2
m=1
QC-gain bandwidth
L_{EC}
$2kL_{EC} = 2\pi m$
$2kL_{EC} + \Phi_{meta} + \pi = 2\pi m$
0
50
100
150
200
250
10 μm
L_{EC} (μm)

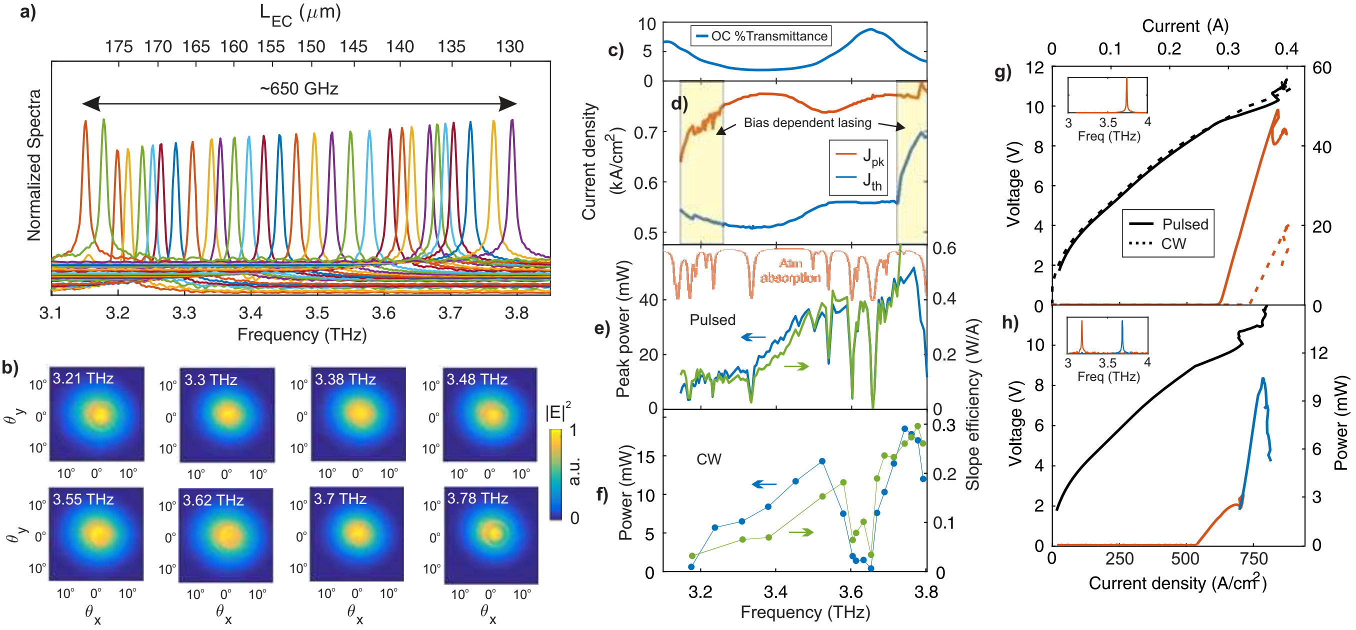
a)
L_EC (μm)
175 170 165 160 155 150 145 140 135 130
~650 GHz
Normalized Spectra
3.1 3.2 3.3 3.4 3.5 3.6 3.7 3.8
Frequency (THz)
b)
3.21 THz
3.3 THz
3.38 THz
3.48 THz
3.55 THz
3.62 THz
3.7 THz
3.78 THz
θy
θx
10° 0° 10°
|E|²
1
a.u.
0
c)
OC %Transmittance
10 5 0
d)
Bias dependent lasing
Current density (kA/cm²)
0.7 0.6 0.5
J_pk
J_th
e)
Atm absorption
Pulsed
Peak power (mW)
40 20 0
Slope efficiency (W/A)
0.6 0.4 0.2 0
f)
CW
Power (mW)
15 10 5 0
0.3 0.2 0.1 0
3.2 3.4 3.6 3.8
Frequency (THz)
g)
Current (A)
0 0.1 0.2 0.3 0.4
Voltage (V)
12 10 8 6 4 2 0
60 40 20 0
Freq (THz)
3 3.5 4
Pulsed
CW
h)
Voltage (V)
10 8 6 4 2 0
Power (mW)
12 9 6 3 0
Freq (THz)
3 3.5 4
0 250 500 750
Current density (A/cm²)

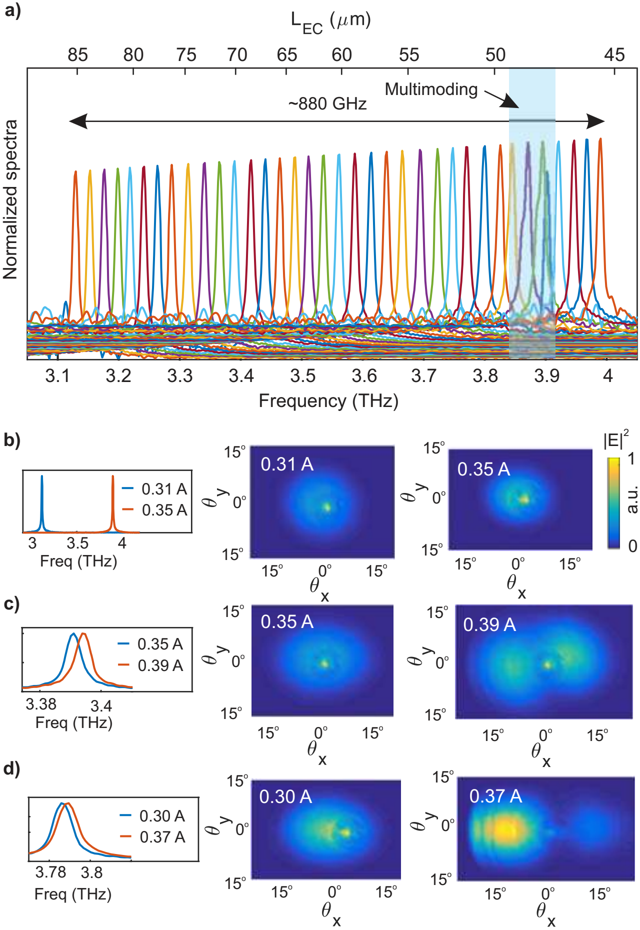
a)
L_EC (μm)
85 80 75 70 65 60 55 50 45
Multimoding
~880 GHz
Normalized spectra
3.1 3.2 3.3 3.4 3.5 3.6 3.7 3.8 3.9 4
Frequency (THz)
b)
0.31 A
0.35 A
3 3.5 4
Freq (THz)
0.31 A
0.35 A
15° 0° 15°
θ_y
θ_x
|E|²
1
a.u.
0
c)
0.35 A
0.39 A
3.38 3.4
Freq (THz)
0.35 A
0.39 A
d)
0.30 A
0.37 A
3.78 3.8
Freq (THz)
0.30 A
0.37 A